JACS
JOURNAL OF THE AMERICAN CHEMICAL SOCIETY
Article
pubs.acs.org/JACS

Two-Electron HCl to H_2 Photocycle Promoted by Ni(II) Polypyridyl Halide Complexes

David C. Powers, Bryce L. Anderson, and Daniel G. Nocera*

Department of Chemistry and Chemical Biology, Harvard University, 12 Oxford Street, Cambridge, Massachusetts 02138, United States

Supporting Information

ABSTRACT: Photochemical HX splitting requires the management of two protons and the execution of multielectron photoreactions. Herein, we report a photoinduced two-electron reduction of a polypyridyl Ni(II) chloride complex that provides a route to H_2 evolution from HCl. The excited states of Ni complexes are too short to participate directly in HX activation, and hence, the excited state of a photoredox mediator is exploited for the activation of HX at the Ni(II) center. Nanosecond transient absorption (TA) spectroscopy has revealed that the excited state of the polypyridine results in a photoreduced radical that is capable of mediating HX activation by producing a Ni(I) center by halogen-atom abstraction. Disproportionation of the photogenerated Ni(I) intermediate affords Ni(II) and Ni(0) complexes. The Ni(0) center is capable of reacting with HX to produce H_2 and the polypyridyl Ni(II) dichloride, closing the photocycle for H_2 generation from HCl.

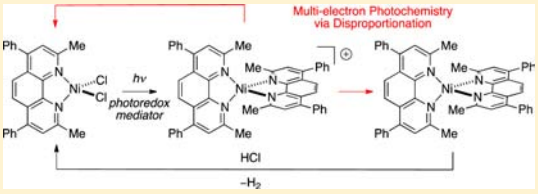

INTRODUCTION

The photodriven splitting of hydrohalic acids (HX) into H_2 and X_2 is a promising approach to storing solar energy in the form of a redox flow battery[1] or chemical fuel.[2] The conversion of HX to H_2 and X_2 stores considerable energy. For the case of X = Cl, HX splitting stores approximately the same amount of energy per electron as the conversion of H_2O to H_2 and $^1/_2O_2$ but only requires the management of two electrons and protons as opposed to the four that are required in water splitting.[3] Despite the imperative of energy storage in its various forms, the molecular details of HX-splitting chemistry has received little attention. Extant HX-splitting photocatalysts are based on precious metals, with a particular emphasis on rhodium and iridium. Dirhodium phosphazane catalysts are especially effective at promoting the photocatalytic evolution of H_2 from HX[4,5] owing to the ability of the diphosphazane ligand to enforce two-electron-mixed valency[3] and to accommodate M(μ^2-X)M−X bridging intermediates from which reductive elimination may occur.[6,7] Studies of these complexes as well as those of Pt and Au reveal that turnover efficiencies are limited by the strong M−X bond,[8−10] which has been proposed to be activated via ligand-to-metal charge transfer (LMCT) excited states.[6,8,9]

The strength of the MX bond may be reduced by moving to first-row transition metals, which possess the added benefit that they are noncritical elements. Our previous efforts to achieve either H_2- or X_2-forming photoreactions with Ni(II) complexes establish that the requisite two-electron chemistry of HX splitting is circumvented by one-electron photoreactions. Photolysis of Ni(II) hydridohalide complex **1**, affords Ni(I) chloride **2** (L = 1,3-dimesitylimidazol-2-ylidene (eq 1)),[11] and photolysis of Ni_2(II,II) complex **3** affords Ni_2(I,I) complex **4** (L′ = 1,3-bis(2,6-diisopropylphenyl)imidazole-2-ylidene (eq 2)),[12] Both Ni(I) complexes **2** and **4** are unreactive toward HCl, precluding an HX splitting cycle from being achieved.

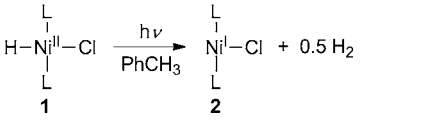

(1)

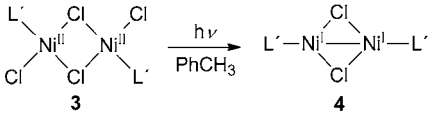

(2)

Figure 1 presents a strategy for an authentic two-electron H_2 photocycle using HX as a substrate. In the case of nickel, driving reductive elimination from a Ni(III) state is preferred over a Ni(II) state based on the facility of two-electron reductive elimination reactions from mononuclear Ni(III) centers, as observed for Ni-catalyzed cross-coupling reactions.[13−18] In principle, a Ni(III)-like state can be accessed from a metal-to-ligand charge transfer (MLCT) of a Ni(II) halide complex. However, whereas long-lived MLCT excited states are frequently encountered in the photochemistry of second- and third-row transition metal complexes, first-row transition metal complexes typically possess extremely short-lived charge transfer states.[19−21] The compression of the crystal field splitting attendant upon moving from a second- to first-row metal results in the placement of d−d ligand-field states to

Received: August 24, 2013
Published: November 18, 2013

   dx.doi.org/10.1021/ja408787k | J. Am. Chem. Soc. 2013, 135, 18876−18883

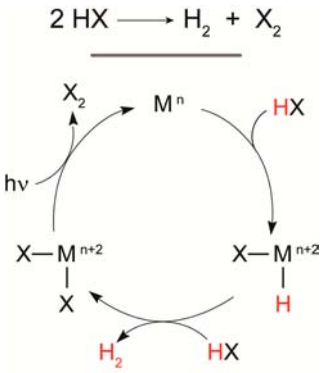

Figure 1. Catalytic cycle for HX splitting. Two-electron photoreduction of a metal dihalide generates an intermediate poised to thermally reduce protons.

lower energy than charge-separated states.[22,23] The consequence of this energetic reordering of excited states can be seen by comparing the lifetimes of charge-separated states of Ru and Fe polypyridyl complexes: Ru^{2+} polypyridyl complexes display charge-separated state lifetimes of 600−850 ns,[24−31] whereas the related Fe^{2+} polypyridyl complexes display charge separated lifetimes on the order of ∼100 fs.[22,23]

In order to overcome the inherently short excited state lifetimes of nickel complexes, we targeted a design strategy in which photochemistry is derived from a photoredox mediator. Pyridine has received substantial attention as a potential small-molecule redox mediator because of the observation that single-electron transfer reactions can interconvert pyridinium ions and pyridinyl radicals.[32] Electrochemical and photoelectrochemical reduction reactions of CO_2 to methanol have been proposed to proceed through pyridinyl radical intermediates, which engage in proton-coupled electron transfer (PCET) reactions to accomplish substrate reduction.[33−35] The role of the electrode surface and the precise pyridine oxidation state are topics of current discussion.[36−38] Using these results as a guidepost, we turned our attention to bipyridine excited states, which are known to engage in H-atom abstraction (HAA) reactions,[39−42] to access a reducing pyridinyl radical for substrate reduction.

We now report a HX-to-H_2 photocycle promoted by a Ni(II)/Ni(0) couple. Reduction of a Ni(II) dihalide complex by a polypyridyl photoredox mediator provides either Ni(I) or Ni(0) complexes dependent on the particular reaction conditions employed. The photogenerated Ni(0) species reacts thermally with HCl to generate H_2 and regenerate the Ni(II) dihalide, demonstrating a closed photocycle for the evolution of H_2 from HCl mediated by an earth-abundant transition metal complex.

EXPERIMENTAL SECTION

General Considerations. All reactions were carried out in an N_2-filled glovebox. Anhydrous solvents were obtained by filtration through drying columns.[43] $NiCl_2$dme (dme = 1,2-dimethoxyethane) and Ni(cod)$_2$ (cod = 1,5-cyclooctadiene) were obtained from Strem Chemicals, while 2,9-dimethyl-4,7-diphenyl-1,10-phenanthroline (bathocuproine, bc), 2,9-dimethyl-1,10-phenanthroline (dmphen), 6,6′-dimethyl-2,2′-bipyridine (dmbpy), and 2,2′-biquinoline (biq) were obtained from Sigma Aldrich. All chemicals were used without purification. $NiCl_2$dmphen (**8**),[44] $NiCl_2$biq (**10**),[44] and Ni(dmphen)$_2$ (**13**)[45] were prepared according to literature procedures.

Physical Methods. NMR spectra were recorded at the Harvard University Department of Chemistry and Chemical Biology NMR facility on a Varian Unity/Inova 500 spectrometer operating at 500 MHz for ^{1}H acquisitions. NMR chemical shifts are reported in ppm with the residual solvent resonance as internal standard. UV−vis spectra were recorded at 293 K in quartz cuvettes on a Spectral Instruments 400 series diode array and were blanked against the appropriate solvent. Solution magnetic moments were determined using the Evans method[46] in 1:1 THF/CH_3CN and measured using ^{19}F NMR (hexafluorobenzene added); diamagnetic corrections were estimated from Pascal constants.[47] Perpendicular mode X-band EPR spectra were recorded on Bruker ElexSys E500 EPR equipped with an N_2 dewer for measurements at 77 K. EPR spectra were referenced to diphenylpicrylhydrazyl, DPPH (g = 2.0037). Spectra were simulated using EasySpin 4.5.0 implemented with MATLAB to obtain g-values. EPR spectra of [**7**]OTf were collected in both 2-methyltetrahydrofuran (2-MeTHF) and 9:1 EtOH/MeOH, and the observed features showed no solvent dependence. Steady-state emission spectra were recorded on an automated Photon Technology International (PTI) QM 4 fluorimeter equipped with a 150 W Xe arc lamp and a Hamamatsu R928 photomultiplier tube.

Steady-state photochemical reactions were performed using a 1000 W high-pressure Hg/Xe arc lamp (Oriel), and the beam was passed through a water-jacketed filter holder containing the appropriate long-pass filter, an iris, and a collimating lens. Nanosecond transient absorption (TA) measurements were made at 10 Hz with the pump light provided by the third harmonic (355 nm) of a Quanta-Ray Nd:YAG laser (Spectra-Physics) or with 310 nm light generated from the frequency doubled 620 nm signal of a Spectra-Physics Quanta-Ray MOPO-700 with FDO-970 option pumped with the 355 nm light from the aforementioned laser. The signal light passed through a Triax 320 spectrometer, where it was dispersed by a 300 groove/mm × 250 nm blazed grating and collected with either an intensified gated CCD camera (ICCD, CCD 30-11, Andor Technology, 1024 × 256 pixels, 26 μm^2) for TA spectra or a photomultiplier tube (PMT) for TA single-wavelength kinetics. PMT outputs were collected and averaged with a 1 GHz oscilloscope (LeCroy 9384CM). A TTL pulse synchronized with the Q-switch of the Infinity laser was delayed 99 ms before triggering the shutter for the probe light. Electronic delays were created with SRS DG535 delay generators (Stanford Research Systems). These delay boxes, in combination with electronic shutters (Uniblitz), were used to create the necessary pulse sequence. THF/CH_3CN (1:1) solutions of complexes **5** and bc were prepared in 50 mL Schlenk flasks in an N_2-filled glovebox. Solutions were flowed through a 3 mm diameter, 1 cm path length flow cell (Starna, type 585.2) using a peristaltic pump and positive argon pressure. Details of picosecond TA spectroscopy can be found in the Supporting Information.

Preparation of Ni(II) Complexes ($LNiCl_2$). *Complex* **5**. To a suspension of $NiCl_2$(dme) (181 mg, 8.23 × 10^{-4} mol, 1.00 equiv) in THF was added bc (297 mg, 8.23 × 10^{-4} mol, 1.00 equiv) as a solid. The mixture was stirred at 23 °C for 10 h, during which time a pink precipitate was observed. The mixture was concentrated to dryness and the residue was washed with THF and dried in vacuo to afford 403 mg of the title complex as a pink solid (96% yield). ^{1}H NMR (500 MHz, THF-d_8) δ (ppm): 80.05 (s, 2H), 28.12 (s, 2H), 18.5 (br s, 6H), 9.61 (d, J = 7.3 Hz, 4H), 8.81 (t, J = 7.3 Hz, 2H), 7.19 (dd, J = 7.3 Hz, J = 7.3 Hz, 4H). μ_{eff} = 3.59 μB. Crystals suitable for single-crystal diffraction analysis were obtained by slow evaporation of a concentrated MeOH solution of the complex.

Complex **9** was prepared analogously: 97% yield. ^{1}H NMR (500 MHz, THF-d_8) δ (ppm): 77.3 (br s, 2H), 63.41 (s, 2H), 27.7 (br s, 6H), 23.07 (s, 2H). μ_{eff} = 3.57 μB. Crystals suitable for single-crystal diffraction analysis were obtained by slow evaporation of a MeOH solution of the complex.

Preparation of Ni(0) Complexes (L_2Ni). *Complex* **6**. To a suspension of Ni(cod)$_2$ (70.0 mg, 2.54 × 10^{-4} mol, 1.00 equiv) in THF was added bc (93.8 mg, 5.09 × 10^{-4} mol, 2.00 equiv) as a solid. The reaction mixture was warmed to 60 °C, at which temperature it was stirred for 12 h. The reaction mixture turned from a pale yellow suspension to an inky purple solution during the course of heating. The reaction mixture was filtered through Celite. The Celite was washed with THF, the filtrate was combined, and solvent was removed

dx.doi.org/10.1021/ja408787k | J. Am. Chem. Soc. 2013, 135, 18876−18883

Table 1. Crystal Data and Structure Refinement

	5	**6**·THF	[**7**]OTf·3THF	[**11**]PF_6	[**12**]ClO_4·bc	**14**·0.5PhH	**15**·THF
formula	$C_{26}H_{20}Cl_2N_2Ni$	$C_{56}H_{48}N_4NiO$	$C_{65}H_{64}F_3N_4NiO_6S$	$C_{28}H_{24}F_6N_4NiP$	$C_{54}H_{36}ClN_6NiO_4$	$C_{39}H_{27}N_4Ni$	$C_{22}H_{21}ClN_2O$
fw, g/mol	490.06	851.70	1144.98	620.19	927.04	610.35	364.86
temp, K	100(2)	110(2)	110(2)	100(2)	100(2)	100(2)	100(2)
cryst system	monoclinic	monoclinic	monoclinic	triclinic	monoclinic	triclinic	triclinic
space group	*P21/c*	*P21/n*	*P21/c*	$P\bar{1}$	*P2/n*	$P\bar{1}$	$P\bar{1}$
color	pink	purple	blue	red-black	purple	blue-green	green
a, Å	13.0496(9)	18.007(3)	17.4078(4)	10.590(3)	13.6604(9)	13.4506(6)	8.6703(15)
b, Å	21.9451(15)	11.3520(17)	11.0915(2)	10.945(3)	11.1003(7)	14.7269(6)	13.872(2)
c, Å	7.8238 (6)	21.176(3)	29.2364(6)	11.849(3)	13.7705(9)	15.8071(7)	15.823(3)
α, deg	90	90	90	76.804(4)	90	88.800(1)	77.753(3)
β, deg	104.450(1)	96.196(3)	90.371(1)	77.027(4)	98.787(1)	67.020(1)	81.643(3)
γ, deg	90	90	90	77.385(4)	90	88.659(1)	75.191(3)
V, A^3	2169.7(3)	4303.3(11)	5644.8(2)	1282.6(6)	2063.4(2)	2881.6(2)	1789.7(5)
Z	4	4	6	2	4	6	2
R1[a]	0.039	0.057	0.052	0.085	0.033	0.039	0.071
wR2[b]	0.098	0.170	0.127	0.277	0.084	0.084	0.187
GOF[c] (F^2)	0.87	1.07	1.05	1.05	1.05	1.02	1.05

[a] $R1 = \sum||F_o| - |F_c||/\sum|F_o|$. [b] $wR2 = (\sum(w(F_o^2 - F_c^2)^2)/\sum(w(F_o^2)^2))^{1/2}$. [c] $GOF = (\sum w(F_o^2 - F_c^2)^2/(n-p))^{1/2}$ where *n* is the number of data and *p* is the number of parameters refined.

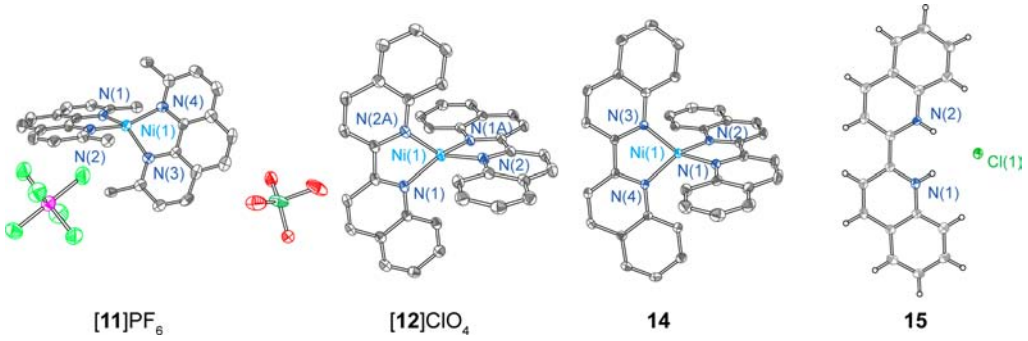

Figure 2. Thermal ellipsoid plots of [**11**]PF_6, [**12**]ClO_4, **14**, and **15**. Except for compound **15**, hydrogen atoms and solvent molecules have been omitted for clarity. Ellipsoids are drawn at the 50% probability level. Thermal ellipsoid plots of **5**, **6**, and [**7**]OTf appear in Figure 3

in vacuo to afford 184 mg of **6** as an air-sensitive dark purple solid (93% yield). ^{1}H NMR (500 MHz, C_6D_6) *δ* (ppm): 7.95 (s, 4H), 7.85 (s, 4H), 7.65 (d, *J* = 7.3 Hz, 8H), 7.36 (t, *J* = 7.3 Hz, 4H), 7.18 (dd, *J* = 7.8 Hz, *J* = 7.8 Hz, 8H), 2.48 (s, 12H). Crystals suitable for single-crystal diffraction analysis were obtained from a THF solution of the complex layered with $PhCH_3$.

Complex ***14*** was prepared analogously: 81% yield. ^{1}H NMR (500 MHz, benzene-d_6) *δ* (ppm): 10.22 (d, *J* = 8.3 Hz, 4H), 9.19 (d, *J* = 8.8 Hz, 4H), 7.56 (d, *J* = 7.8 Hz, 4H), 7.29 (t, *J* = 7.3 Hz, 4H), 7.15 (overlap with solvent signal, 4H), 6.80 (d, *J* = 8.8 Hz, 4H). Crystals suitable for single-crystal diffraction analysis were obtained from a THF solution of the complex layered with $PhCH_3$.

Preparation of Ni(I) Complexes ($L_2Ni^+X^-$). *Complex [7]OTf.* To a solution of $Ni(bc)_2$ (**6**) (59.0 mg, 7.57×10^{-5} mol, 1.00 equiv) in THF was added AgOTf (19.5 mg, 7.57×10^{-5} mol, 1.00 equiv) as a suspension in THF. The reaction solution immediately turned from dark purple to blue. The reaction mixture was stirred at 23 °C for 30 min before being filtered through Celite. The filtrate was concentrated in vacuo and the residue was taken up in 1:1 THF/pentane. Complex [**7**]OTf was isolated by filtration to afford 55.1 mg of an air-sensitive dark blue solid (80% yield). ^{1}H NMR (500 MHz, THF-d_8) *δ* (ppm): 33.8 (br s, 4H), 12.51 (s, 4H), 8.00−7.96 (m, 12H), 7.07 (s, 8H), 0.8 (br s, 12H). EPR (9:1 EtOH/MeOH) *g*-value: g_1 = 2.4524; g_2 = 2.2039; g_3 = 2.1655. μ_{eff} = 2.46 *μ*B.

Complexes [11]PF_6 and [12]ClO_4 were prepared analogously. Complex [**11**]PF_6: 82% yield. ^{1}H NMR (500 MHz, CD_3CN) *δ* (ppm): 33.0 (br s, 4H), 13.3 (s, 4H), 11.6 (br s, 4H), 0.4 (br s, 12H). μ_{eff} = 2.53 *μ*B. EPR (9:1 EtOH:MeOH) *g*-value: g_1 = 2.4616; g_2 = 2.2004; g_3 = 2.1626. Crystals suitable for single-crystal diffraction analysis were obtained from a MeOH solution of the complex. Complex [**12**]ClO_4: 74% yield. ^{1}H NMR (500 MHz, CD_3CN) *δ* (ppm): 20.4 (br s, 4H), 19.7−19.4 (m, 12H), 10.7 (br s, 4H), 8.0 (s, 4H). Crystals suitable for single-crystal diffraction analysis were obtained from a MeOH solution of the complex.

Preparation of K·biq. To a solution of biq (250 mg, 9.72×10^{-4} mol, 1.00 equiv) in THF was added potassium (38.0 mg, 9.72×10^{-4} mol, 1.00 equiv) as a solid. The reaction mixture was stirred at 23 °C for 4 h, during which time the reaction mixture assumed a dark red-brown color. The reaction mixture was filtered through Celite and the filtrate was concentrated in vacuo to afford 55.1 mg of the title complex as an air-sensitive dark red-brown solid (94% yield). Treatment of K·biq with HCl·dioxane in THF results in immediate color change of the reaction solutions from red-brown to green. Removal of solvent in vacuo affords **15** as a green solid (71%). Crystals suitable for single-crystal diffraction analysis were obtained from a THF solution of the compound.

X-ray Crystallographic Details. All structures were collected on a Bruker three-circle platform goniometer equipped with an Apex II CCD and an Oxford cryostream cooling device at 100 K. Radiation was generated from a graphite fine focus sealed tube Mo K*α* (0.710 73 Å) source. Crystals were mounted on a cryoloop or glass fiber pin using Paratone N oil. Data were integrated using SAINT and scaled with either a numerical or multiscan absorption correction using SADABS. The structures were solved by direct methods using SHELXS-97 and refined against F^2 on all data by full matrix least-squares with SHELXL-97. All non-hydrogen atoms were refined

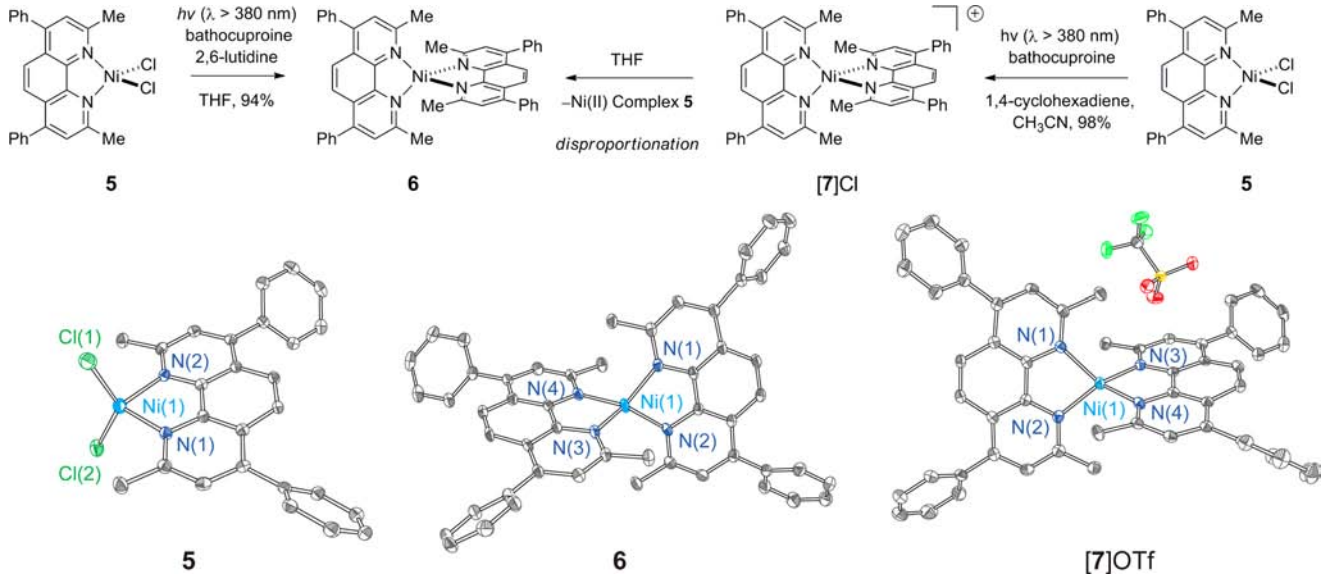

Figure 3. Photolysis of Ni(II) complex **5** in THF afforded Ni(0) complex **6**, while photolysis of **5** in CH_3CN/1,4-cyclohexadiene afforded Ni(I) complex [7]Cl. Thermal ellipsoid plots of **5**, **6**, and [7]OTf are shown. Ellipsoids are drawn at the 50% probability level.

anisotropically. Hydrogen atoms were placed at idealized positions and refined using a riding model. Crystal data and refinement statistics are summarized in Table 1, and thermal ellipsoid plots are collected in Figures 2 and 3.

RESULTS AND DISCUSSION

Synthesis and Steady-State Photochemistry. Treatment of $NiCl_2$dme with bathocuproine (bc) afforded pink Ni(II) dichloride complex **5**, which is pseudo-tetrahedral in the solid state and in solution. THF solutions of **5** exhibit a UV–vis absorption spectrum that features d–d absorptions at 500, 852, and 1005 nm (ε = 200, 70, and 100 M^{-1} cm^{-1}, respectively). Referenced to T_d symmetry, the d–d transitions arise from $^3T_1$ to $^3A_2$ and $^3T_2$ excitations;[48,49] the deviation of **5** from T_d symmetry gives rise to multiple transitions for each of these absorption manifolds.[50] The room-temperature magnetic moment, measured by the Evans method, was determined to be μ_{eff} = 3.6.[51] Photolysis (λ > 305 nm) of **5** in THF in the presence of both 2.0 equiv of 2,6-lutidine and 2.0 equiv of exogenous bc caused the pale pink reaction solution to turn dark purple (Figure 4a). The dark purple product was identified as the Ni(0) complex **6** by comparison of the UV–vis and ^1H NMR spectra of the photochemical reaction mixture to a spectrum obtained for an authentic sample of **6**, which was prepared by treatment of $Ni(cod)_2$ with 2.0 equiv of bc. The central C–C bond of the phenanthroline backbone (C^2–$C^{2'}$ in bipyridine numbering) contracts from 1.441(4) Å in **5** to 1.411(5) Å in **6**. For comparison, the corresponding bond in free bc is 1.46 Å.[52] Both the dark purple color and the C–C bond contraction[53] in **6** are consistent with substantial redox noninnocence of the bc ligands in **6**, suggesting **6** may be described as a Ni(II) complex with two pendent ligand-based radicals.

In contrast to the photolysis of **5** in THF, when Ni(II) complex **5** is photolyzed in CH_3CN in the presence of exogenous bc and 1,4-cyclohexadiene added as an H-atom donor (vide infra), a dark blue solution is obtained (Figure 4b). The identity of the blue photoproduct was established to be homoleptic Ni(I) complex [7]Cl by comparison of the photochemical reaction mixture with the spectral data of

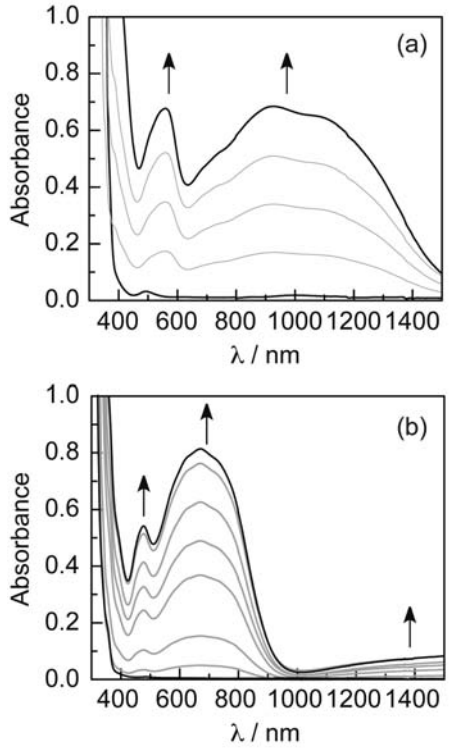

Figure 4. Spectral evolution during photolysis (λ > 305 nm) of (a) Ni(II) complex **5** to Ni(0) complex **6** in THF and (b) Ni(II) complex **5** to Ni(I) complex [7]Cl in 1:1 CH_3CN/1,4-cyclohexadiene.

independently prepared [7]OTf, which was obtained by treatment of Ni(0) complex **6** with AgOTf. ^1H NMR, EPR, and electronic absorption spectroscopies were used to assign the structure of [7]OTf. X-ray crystallographic analysis of a single crystal established the structure of [7]OTf to be the homoleptic Ni(I) structure drawn in Figure 3. The central C–C bond of [7]OTf was measured to be 1.429(4) Å, which is between the distances in Ni(0) complex **6** (C–C = 1.411(5) Å) and Ni(II) complex **5** (C–C = 1.441(4) Å).

dx.doi.org/10.1021/ja408787k | J. Am. Chem. Soc. 2013, 135, 18876–18883

The disparate, solvent-dependent photoreactivity of **5**, which undergoes either one- or two-electron photoreduction depending on the reaction solvent, was probed by examining the solvent-dependent behavior of the isolated Ni(I) complexes. The results of these experiments are summarized in Figure 5.

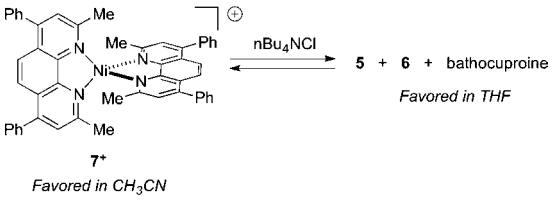

Figure 5. Solvent-dependent equilibrium favors Ni(I) complex 7^+ in CH_3CN, while Ni(II) and Ni(0) complexes **5** and **6** are favored in THF.

Treatment of Ni(0) complex **6** with AgOTf affords Ni(I) complex [**7**]OTf, which is stable in both THF and CH_3CN. Treatment of a THF solution of [**7**]OTf with 1.0 equiv of *n*-Bu_4NCl prompted immediate disproportionation of 7^+ to Ni(II) complex **5** and Ni(0) complex **6**, with concurrent liberation of 0.5 equiv of bc (see Figure S9 in Supporting Information for ^1H NMR). In contrast, [**7**]Cl is stable with respect to disproportionation in CH_3CN; treatment of [**7**]OTf with 1.0 equiv of *n*-BuN_4Cl in CH_3CN did not result in the observation of either **5** or **6** (Figure S10). The observation of solvent-dependent disproportionation of 7^+ in the presence of Cl^- clarifies the observation of **6** from photolysis of **5** in THF and the observation of 7^+ from photolysis of **5** in CH_3CN. Solvent-dependent, chloride-induced disproportionation is also observed in photochemical reactions; concentration of the blue photoreaction mixture of Ni(I) complex [**7**]Cl produced by photolysis in CH_3CN and 1,4-cyclohexadiene and redissolution in THF affords a purple solution of **5** and **6**.

The effect of bis-imine ligand on the efficiency of photoreduction was probed using $NiCl_2$dmphen (**8**), $NiCl_2$dmbpy (**9**), and $NiCl_2$biq (**10**) (Figure 6). Both

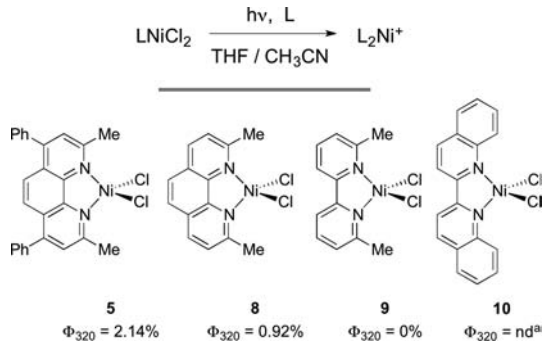

Figure 6. Quantum yield for photoreduction of Ni(II) complexes is correlated with reduction potential of the bis-imine ligand. Insolubility of **10** prevented determination of quantum yield.

$NiCl_2$dmphen (**8**) and $NiCl_2$biq (**10**) participate in photoreduction chemistry in analogy to complex **5** (Figures S22–S24). In addition, isolated mononuclear Ni(I) complexes $Ni(dmphen)_2PF_6$ ([**11**]PF_6) and $Ni(biq)_2PF_6$ ([**12**]PF_6) exhibit chloride-induced disproportionation in THF to afford $Ni(dmphen)_2$ **13** and **8** or $Ni(biq)_2$ (**14**) and **10**, respectively. In contrast to complexes **5** and **8**, regardless of the wavelength of irradiation employed, $NiCl_2$dmbpy (**9**) is not photoreduced (Figure S25). The effect of ligand structure on photoreduction efficiency was probed by comparison of the quantum yields for one-electron photoreduction of complexes **5**, **8**, and **9**. Whereas complexes **5**, **8**, and **9** are isostructural in solution, established by both solution magnetic moment (**5**, μ_{eff} = 3.6; **8**, μ_{eff} = 3.5; **9**, μ_{eff} = 3.6) and similarity of d–d transitions (Figure S18), their photochemical quantum yields are 2.14% (**5**), 0.92% (**8**), and 0% (**9**). This trend follows the expected ease of reduction of the ancillary polypyridyl ligand; while electrochemical reduction of bipyridine derivatives is frequently irreversible, monoprotonated bipyridines display the anticipated substituent-dependent redox potentials.[54,55] The quantum yield for photoreduction of biquinoline-supported Ni(II) complex **10** could not be determined because of insolubility of **10** under photoreduction conditions.

Thermally Promoted Proton Reduction Reactions. With conditions in hand to achieve the two-electron photoreduction of Ni(II) chlorides, we examined the viability of proton reduction by the reduced Ni complexes. Treatment of Ni(0) complexes **6** and **13** with HCl in MeOH generates H_2 in 60 and 85% yield, respectively, along with Ni(II) complex **5** and **8**; the results of these experiments are summarized in Figure 7.

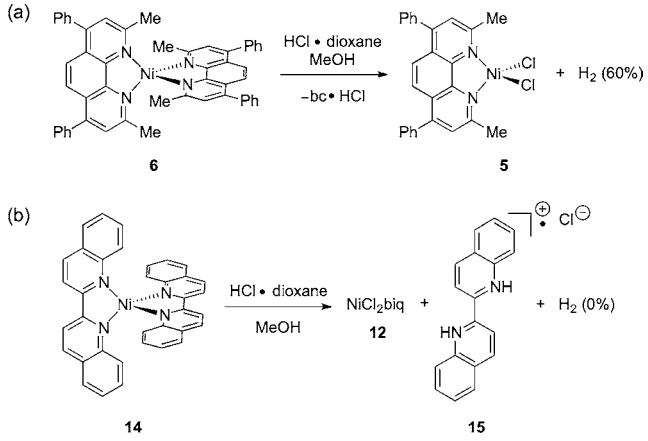

Figure 7. (a) Protonation of Ni(0) complex **6** affords Ni(II) chloride **5**, as well as H_2. (b) Protonation of Ni(0) complex **14** affords Ni(II) chloride **12** together with pyridinyl radical **15** but no H_2.

The H_2 yields were determined by GC analysis and confirmed by independent Toepler pump combustion analysis (Figure S36). Formation of **5** and **8** following H_2 evolving reactions of **6** and **13**, respectively, establishes a closed H_2-evolving photocycle using an earth-abundant transition metal complex. While **5** is thermally stable to HCl, photolysis of **5** in the presence of protons leads to the loss of bc and <0.2 turnover of H_2 production.

The ligand requirements for a complex that can mediate both oxidative and reductive half reactions of HX splitting are strict. A closed photocycle cannot be achieved for 2,2′-biquinoline complex **10**. Whereas protonation of $Ni(biq)_2$ (**14**) affords Ni(II) complex **10**, no H_2 is observed. Instead of generating H_2, the reducing equivalents incipient in Ni(0) complex **14** promote the reduction of biq to afford pyridinium-stabilized pyridinyl radical **15**. Radical **15** could also be synthesized by sequential treatment of biq with K^0 and HCl and features a $d(C^2–C^2)'$ of 1.435(6) Å, diagnostic of a monoreduced biquinoline[56] (compared to $d(C^2–C^2)'$ in 2,2′-biquinoline of 1.492(3) Å[57]). Neither thermolysis or photolysis of **15** liberates H_2. Similar ligand reduction chemistry has not been observed in

dx.doi.org/10.1021/ja408787k | J. Am. Chem. Soc. 2013, 135, 18876–18883

the protonation of **6** but may account for the nonquantitative yield of H_2 observed. Although photoreduction of Ni(II) complexes supported by bipyridine ligands is promoted by more reducing ligands, the extent of proton reduction is limited by deleterious ligand reduction processes.

Time-Resolved Photochemical Experiments. In order to probe our contention that photogenerated pyridinyl radicals could mediate the requisite photoreduction chemistry, a nanosecond transient absorption (TA) spectrum of a solution of bc was recorded. The collected TA spectrum featured a growth centered at 526 nm (Figure 8a). We assign the transient

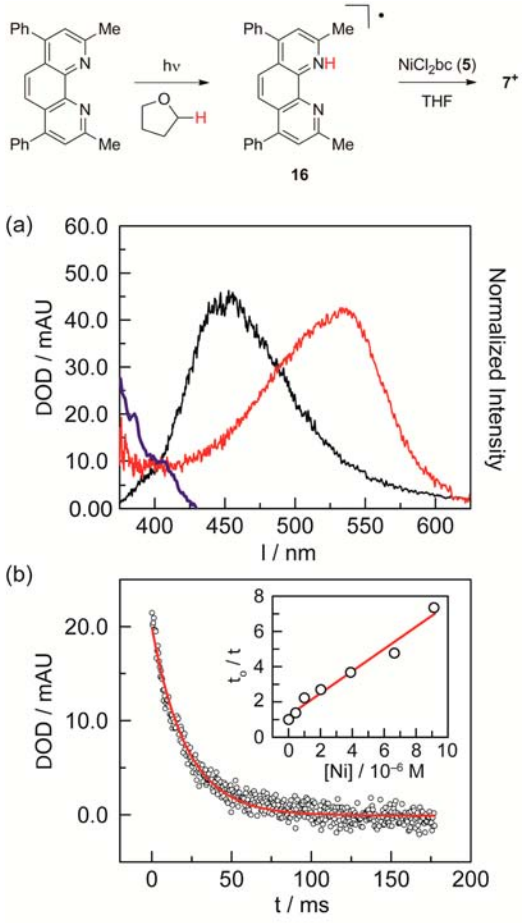

Figure 8. (a) Transient absorption spectrum (red) obtained by laser flash photolysis (355 nm pump) of a 1:1 THF/CH_3CN solution of bc, recorded at 40 ns delay: normalized absorption (blue) and emission (black) spectra of bc. (b) Single wavelength (526 nm) kinetic decay of transient intermediate. Inset: plot of τ_o/τ vs [**5**].

species as ligand radical **16**, based on the TA spectra obtained upon flash photolysis of bipyridines, which also are ascribed to pyridinyl radicals generated by hydrogen-atom abstraction (HAA) reactions from solvent by electronically excited bipyridines.[39−42] HAA abstraction from THF generates an equivalent of furanyl radical, which can participate in a variety of subsequent transformations.[58,59] The intensity of the TA signal at 526 nm is stronger in THF than in CH_3CN, and no TA signal is observed in hexane (Figure S27), which is consistent with the relative H-atom donor capacities of these solvents. Monitoring the decay of **16** at 526 nm provided a lifetime of 21.66 ± 0.43 μs (Figure 8b). The lifetime of **16** was diminished in the presence of Ni(II) complex **5**; a plot of τ_o/τ vs [**5**] is linear, consistent with Stern−Volmer kinetics and with a reaction between transient radical **16** and **5** (Figure 8b, inset). The calculated bimolecular rate constant of 3.0×10^9 M^{-1} s^{-1} is near the diffusion limit.[60]

The dynamics of the photochemistry of bc were probed with ultrafast TA spectroscopy, which revealed two kinetic domains in the evolution of **16**. An initially formed signal, assigned as ^{1}bc* (λ_{max} = 565 nm) generated by n → π* excitation, evolves without well-defined isosbestic points during the first 600 ps following the laser pulse. On the basis of analogy to ultrafast studies of 4,4′-bipyridine, we propose that this initial period involves both HAA from ^{1}bc* to afford **16** and intersystem crossing to generate ^{3}bc* (Figure S35a).[39] Between 600 ps and 3 ns after the laser pulse, the observed TA spectrum evolves with tightly anchored isosbestic points to generate **16** (Figure S35b). Excited state dynamics are finished, and pyridinyl radical **16** is formed within 3 ns of the laser pulse. In contrast to the relatively slow excited-state dynamics observed for bc, ultrafast TA spectra obtained by flash laser photolysis of Ni(II) complex **5** confirm the expectation of fast excited-state dynamics for first-row transition metal polypyridyls. A TA feature as 560 nm is observed for complex **5** and decays to baseline within 15 ps of the laser pulse (Figure 9).

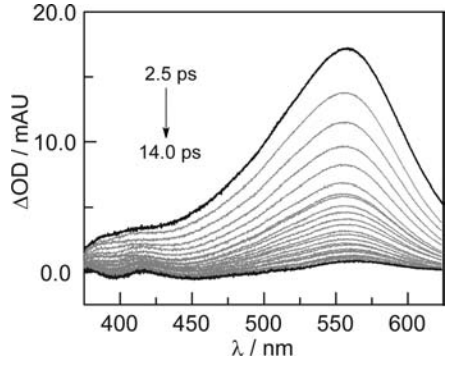

Figure 9. Ultrafast dynamics of laser flash photolysis of Ni(II) complex **5**.

Nanosecond TA spectra were also obtained for dmphen and dmbpy. Flash laser photolysis of dmbpy revealed a feature centered at 370 nm (Figure S31). Unlike the TA spectrum of bc, the intensity of the observed feature in the TA spectrum of dmbpy did not display significant solvent dependence between THF and hexane. This observation, coupled with the similarity of the observed TA signal to a reported TA spectrum of the long-lived triplet excited state of 2,2′-bipyridine,[61] suggests that the observed TA spectrum arises from ^{3}dmbpy*, not a pyridinyl radical. The lifetime of ^{3}dmbpy* was quenched in the presence of Ni(II) complex **9**, but no photoreduction was observed, demonstrating that triplet−triplet annihilation does not lead to reduction of Ni(II). The TA spectrum of dmphen displays a feature centered at 440 nm (Figure S30), which correlates well to a reported spectrum of ^{3}phen*.[62] Unlike the TA spectrum obtained by flash laser photolysis of dmbpy, the intensity of the feature at 440 nm does display solvent dependent intensity; the intensity in hexane is ∼75% the intensity in THF. We do not observe a feature attributable to the monoreduced ligand, but given the observed difference in the intensity and the observation that the triplet excited state of bipyridine is incompetent to accomplish reduction of Ni(II), we propose that the observed photoreduction of Ni(II) complex **8** is

dx.doi.org/10.1021/ja408787k | J. Am. Chem. Soc. 2013, 135, 18876−18883

mediated by pyridinyl radicals. Consistent with the observations regarding solvent-dependent generation of pyridinyl radical intermediates, steady-state photolysis of **5** in either CH_3CN or hexanes (poor H-atom donors) resulted in no photoreduction. Because the reducing pyridinyl radicals are ultimately derived from H-atom abstraction from solvent, the resultant photocycle produces equivalent solvent oxidation byproducts.

Attempts to isolate the product of one-electron reduction of phenanthroline derivatives—either bc or dmphen—did not afford isolable products. Treatment of biq with K^0 provided access to a biquinoline radical anion. The viability of Ni(II) reduction mediated by ligand radicals was confirmed by treatment of Ni(II) complex **10** with K·biq, which afforded Ni(0) complex **14** (Figure 10).

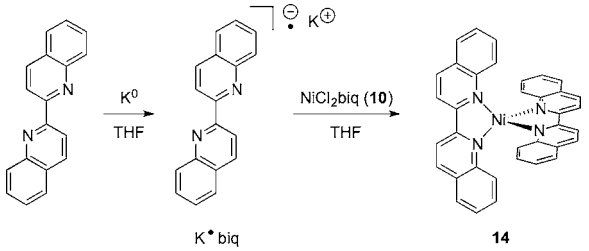

Figure 10. Treatment of Ni(II) complex **10** with stable ligand−radical K·biq affords Ni(0) complex **14**.

CONCLUDING REMARKS

Photocycles for H_2 evolution from HCl require management of multiproton coupled electron transfer reaction (multi-PCET) events. HX-splitting photocatalysis has been achieved by taking advantage of the propensity of second- and third-row transition metals to participate in two-electron reactions. Similar HX-splitting photocycles have not been developed with first-row transition metal complexes. In addition to the facility of one-electron processes at first-row transition metal complexes, extremely short charge-separated state lifetimes are a challenge that needs to be addressed in order to achieve controlled multi-PCET photoreduction reactions. To address the problems of one-electron redox transformations and short charge-separated state lifetimes, we have targeted using photoredox mediators such that the excited state lifetime of interest can be independently tuned, as well as complexes in which one-electron photoreduction is coupled to a disproportionation reaction to enforce the requisite multielectron redox chemistry.

On the basis of the demonstrated ability of pyridine derivatives to serve as one-electron shuttles in proton and CO_2 reduction cycles and the expectation that bipyridine excited states could participate in HAA reactions to generate the requisite reducing pyridinyl radicals, we targeted bipyridines as photoredox mediators for the reduction of Ni(II) complexes. Following this stratagem, we have defined the photocycle shown in Figure 11 for photogeneration of H_2 from HCl mediated by earth-abundant Ni complexes. Ni(II) complex **5**, supported by a bathocuproine ligand, undergoes solvent-dependent photoreduction to either Ni(I) complexes (7^+) or Ni(0) complexes (**6**). Selectivity between one- and two-electron photoreduction was determined to arise from solvent-dependent chloride-ion-induced disproportionation. The proposed role of bipyridine as a photoredox mediator was probed via a series of transient absorption (TA) experiments. The excited state lifetime of Ni(II) complex **5** was found to be

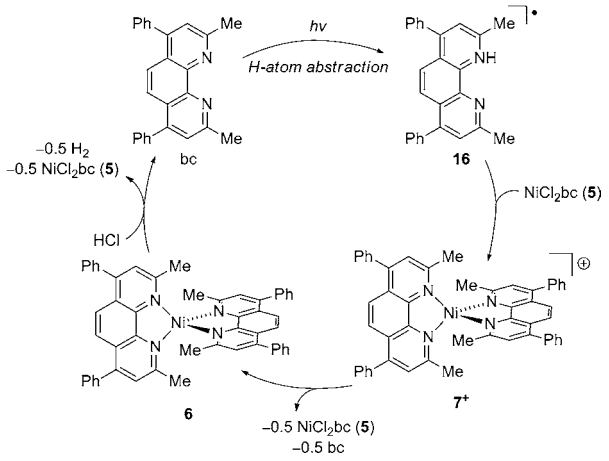

Figure 11. H_2-evolution cycle based on bipyridine photoredox chemistry to generate H_2 from HCl.

extremely short; ultrafast measurements revealed an excited state that decayed to baseline in 15 ps. Nevertheless, laser flash photolysis of bc revealed the presence of a long-lived photogenerated intermediate, assigned to pyridinyl radical **16** based on solvent-dependent yields of **16** as well as on comparison of the TA spectrum of bc to previously reported TA spectra of similar bipyridines. Monitoring the lifetime of pyridinyl radical **16** as a function of [**5**] revealed that the lifetime of radical **16** is quenched by Ni(II) complex **5**. We have directly verified the viability of free ligand radicals to mediate Ni-centered reduction by treatment of Ni(II) complex **10** with K·biq, which results in the observation of Ni(0) complex **14**. A closed photocycle for H_2 evolution from HCl is thus established by protonation of photogenerated Ni(0) complex **6** with HCl, which generates **5** and H_2. These results presented herein thus demonstrate the feasibility of utilizing first-row transition metal complexes to couple two-electron photoreduction reactions and H_2-evolving proton reduction reactions.

ASSOCIATED CONTENT

Supporting Information

Detailed experimental procedures, spectroscopic data for all new compounds, and X-ray crystal data for complex [**11**]PF_6; crystallographic information in txt format. This material is available free of charge via the Internet at http://pubs.acs.org. X-ray data have been deposited in the Cambridge Crystal Structure Database as entries 933283 (**5**), 933284 (**6**), 933285 (**9**), 933286 ([**11**]PF_6), 933287 ([**11**]ClO_4), 936146 ([**12**]-ClO_4), 936147 (**14**), and 936149 (**15**).

AUTHOR INFORMATION

Corresponding Author

dnocera@fas.harvard.edu

Notes

The authors declare no competing financial interest.

ACKNOWLEDGMENTS

We gratefully acknowledge Matt B. Chambers, Thomas S. Teets, and Andrew M. Ullman for helpful discussions, Shao-Liang Zheng and Tamara M. Powers for X-ray crystallography assistance, and the NSF for funding (Grant CHE-1332783).

D.C.P. is supported by a Ruth L. Kirchenstein National Research Service award (Grant F32GM103211).

REFERENCES

(1) Yang, Z.; Zhang, J.; Kintner-Meyer, M. C. W.; Lu, X.; Choi, D.; Lemmon, J. P.; Liu, J. *Chem. Rev.* **2011**, *111*, 3577−3613.
(2) Esswein, A. J.; Nocera, D. G. *Chem. Rev.* **2007**, *107*, 4022−4047.
(3) Nocera, D. G. *Inorg. Chem.* **2009**, *48*, 10001−10017.
(4) Heyduk, A. F.; Nocera, D. G. *Science* **2001**, *293*, 1639−1641.
(5) Elgrishi, N.; Teets, T. S.; Chambers, M. B.; Nocera, D. G. *Chem. Commun.* **2012**, *48*, 9474−9476.
(6) Powers, D. C.; Chambers, M. B.; Teets, T. S.; Elgrishi, N.; Anderson, B. L.; Nocera, D. G. *Chem. Sci.* **2013**, *4*, 2880−2885.
(7) Gray, T. G.; Veige, A. S.; Nocera, D. G. *J. Am. Chem. Soc.* **2004**, *126*, 9760−9768.
(8) Cook, T. R.; Surendranath, Y.; Nocera, D. G. *J. Am. Chem. Soc.* **2009**, *131*, 28−29.
(9) Cook, T. R.; Esswein, A. J.; Nocera, D. G. *J. Am. Chem. Soc.* **2007**, *129*, 10094−10095.
(10) Teets, T. S.; Nocera, D. G. *J. Am. Chem. Soc.* **2009**, *131*, 7411−7420.
(11) Lee, C. H.; Cook, T. R.; Nocera, D. G. *Inorg. Chem.* **2011**, *50*, 714−716.
(12) Lee, C. H.; Lutterman, D. A.; Nocera, D. G. *Dalton Trans.* **2013**, *42*, 2355−2357.
(13) Coronas, J. M.; Muller, G.; Rocamora, M. *J. Organomet. Chem.* **1986**, *301*, 227−236.
(14) Ceder, R. M.; Granell, J.; Muller, G.; Font-Bardía, M.; Solans, X. *Organometallics* **1986**, *15*, 4618−4624.
(15) Higgs, A. T.; Zinn, P. J.; Simmons, S. J.; Sanford, M. S. *Organometallics* **2009**, *28*, 6142−6144.
(16) Tsou, T. T.; Kochi, J. K. *J. Am. Chem. Soc.* **1979**, *101*, 7547−7560.
(17) Matsunaga, P. T.; Hillhouse, G. L.; Rheingold, A. L. *J. Am. Chem. Soc.* **1993**, *115*, 2075−2077.
(18) Koo, K.; Hillhouse, G. L. *Organometallics* **1995**, *14*, 4421−4423.
(19) McCusker, J. K. *Acc. Chem. Res.* **2003**, *36*, 876−887.
(20) Juban, E. A.; Smeigh, A. L.; Monat, J. E.; McCusker, J. K. *Coord. Chem. Rev.* **2006**, *250*, 1783−1791.
(21) Creutz, C.; Chou, M.; Netzel, T. L.; Okumura, M.; Sutin, N. *J. Am. Chem. Soc.* **1980**, *102*, 1309−1319.
(22) Monat, J. E.; McCusker, J. K. *J. Am. Chem. Soc.* **2000**, *122*, 4092−4097.
(23) Ferrere, S.; Gregg, B. A. *J. Am. Chem. Soc.* **1998**, *120*, 843−844.
(24) Caspar, J. V.; Meyer, T. J. *J. Am. Chem. Soc.* **1983**, *105*, 5583−5590.
(25) Balzani, V.; Bolletta, F.; Gandolfi, M. T.; Maestri, M. *Top. Curr. Chem.* **1978**, *75*, 1−64.
(26) Kavarnos, G. J.; Turro, N. J. *Chem. Rev.* **1986**, *86*, 401−449.
(27) Treadway, J. A.; Loeb, B.; Lopez, R.; Anderson, P. A.; Keene, F. R.; Meyer, T. J. *Inorg. Chem.* **1996**, *35*, 2242−2246.
(28) Damrauer, N. H.; Boussie, T. R.; Devenney, M.; McCusker, J. K. *J. Am. Chem. Soc.* **1997**, *119*, 8253−8268.
(29) Damrauer, N. H.; Weldon, B. T.; McCusker, J. K. *J. Phys. Chem. A* **1998**, *102*, 3382−3397.
(30) Damrauer, N. H.; McCusker, J. K. *Inorg. Chem.* **1999**, *38*, 4268−4277.
(31) Strouse, G. F.; Schoonover, J. R.; Duesing, R.; Boyde, S.; Jones, W. E., Jr.; Meyer, T. J. *Inorg. Chem.* **1995**, *34*, 473−487.
(32) Yasukouchi, K.; Taniguchi, I.; Yamaguchi, H.; Shiraishi, M. *J. Electroanal. Chem.* **1979**, *105*, 403−408.
(33) Seshadri, G.; Lin, C.; Bocarsly, A. B. *J. Electroanal. Chem.* **1994**, *372*, 145−150.
(34) Barton, E. E.; Rampulla, D. M.; Bocarsly, A. B. *J. Am. Chem. Soc.* **2008**, *130*, 6342−6344.
(35) Cole, E. B.; Lakkaraju, P. S.; Rampulla, D. M.; Morris, A. J.; Abelev, E.; Bocarsly, A. B. *J. Am. Chem. Soc.* **2010**, *132*, 11539−11551.
(36) Keith, J. A.; Carter, E. A. *J. Am. Chem. Soc.* **2012**, *134*, 7580−7583.
(37) Keith, J. A.; Carter, E. A. *Chem. Sci.* **2013**, *4*, 1490−1496.
(38) Lim, C.-H.; Holder, A. M.; Musgrave, C. B. *J. Am. Chem. Soc.* **2013**, *135*, 142−154.
(39) Buntinx, G.; Naskrecki, R.; Poizat, O. *J. Phys. Chem.* **1996**, *100*, 19380−19388.
(40) Poizat, O.; Buntinx, G.; Valat, P.; Wintgens, V.; Bridoux, M. *J. Phys. Chem.* **1993**, *97*, 5905−5910.
(41) Enomoto, K.; LaVerne, J. A. *J. Phys. Chem. A* **2008**, *112*, 12430−12436.
(42) Castellà-Ventura, M.; Kassab, E.; Buntinx, G.; Poizat, O. *Phys. Chem. Chem. Phys.* **2000**, *2*, 4682−4689.
(43) Pangborn, A. B.; Giardello, M. A.; Grubbs, R. H.; Rosen, R. K.; Timmers, F. J. *Organometallics* **1996**, *15*, 1518−1520.
(44) Butcher, R. J.; Sinn, E. *Inorg. Chem.* **1977**, *16*, 2334−2343.
(45) Fischer, R.; Langer, J.; Malassa, A.; Walther, D.; Görls, H.; Vaughan, G. *Chem. Commun.* **2006**, 2510−2512.
(46) Evans, D. F. *J. Chem. Soc.* **1959**, 2003−2005.
(47) Bain, G. A.; Berry, J. F. *J. Chem. Educ.* **2008**, *85*, 532−536.
(48) Benson, E. E.; Rheingold, A. L.; Kubiak, C. P. *Inorg. Chem.* **2010**, *49*, 1458−1464.
(49) Donoghue, J. T.; Drago, R. S. *Inorg. Chem.* **1962**, *1*, 866−872.
(50) Drago, R. S. *Phyiscal Methods for Chemists*, 2nd ed.; Surfside Scientific Publishers: Gainesville, FL, 1992; p 422.
(51) Cotton, F. A.; Wilkinson, G.; Murillo, C. A.; Bochmann, M. *Advanced Inorganic Chemistry*, 6th ed.; Wiley: New York, 1999; p 840.
(52) Wang, J.; Ye, J.-W.; Wang, Y. *Acta Crystallogr. E* **2007**, *63*, O2007−O2008.
(53) Scarborough, C. C.; Sproules, S.; Weyhermüller, T.; DeBeer, S.; Wieghardt, K. *Inorg. Chem.* **2011**, *50*, 12446−12462.
(54) Tokel-Takvoryan, N. E.; Hemingway, R. E.; Bard, A. J. *J. Am. Chem. Soc.* **1973**, *95*, 6582−6589.
(55) Krishnan, C. V.; Creutz, C.; Schwarz, H. A.; Sutin, N. *J. Am. Chem. Soc.* **1983**, *105*, 5617−5623.
(56) Piglosiewicz, I. M.; Beckhaus, R.; Wittstock, G.; Saak, W.; Haase, D. *Inorg. Chem.* **2007**, *46*, 7610−7620.
(57) Folting, K.; Merritt, L. L., Jr. *Acta Crystallogr.* **1977**, *B33*, 3540−3542.
(58) Wallace, T. J.; Gritter, R. J. *J. Org. Chem.* **1962**, *27*, 3067−3071.
(59) Mignani, S.; Beaujean, M.; Janousek, Z.; Merenyi, R.; Viehe, H. G. *Tetrahedron* **1981**, *37*, 111−115.
(60) Turro, N. J. *Modern Molecular Photochemistry*; University Science Books: Sausalito, CA, 1991; p 314.
(61) Poizat, O.; Buntinx, G. *J. Photochem. Photobiol., A* **2007**, *192*, 172−178.
(62) Bandyopadhyay, B. N.; Harriman, A. *J. Chem. Soc., Faraday Trans.* **1976**, 663−674.